Journal of Biomolecular NMR (2005) 32: 295–308
DOI 10.1007/s10858-005-0659-x

Article

Residue specific ribose and nucleobase dynamics of the cUUCGg RNA tetraloop motif by NMR ^{13}C relaxation

Elke Duchardt & Harald Schwalbe*
Institute for Organic Chemistry and Chemical Biology, Center for Biomolecular Magnetic Resonance, Johann Wolfgang Goethe-University Frankfurt, Marie-Curie Str. 11, D-60439, Frankfurt/Main

Received 7 May 2005; Accepted 10 June 2005

Key words: ^{13}C relaxation, cUUCGg tetraloop motif, diffusion anisotropy, model-free analysis, nucleic acid dynamics

Abstract

The dynamics of the nucleobase and the ribose moieties in a 14-nt RNA cUUCGg hairpin-loop uniformly labeled with ^{13}C and ^{15}N were studied by ^{13}C spin relaxation experiments. R_1, $R_{1\rho}$ and the ^{13}C-{^{1}H} steady-state NOE of C_6 and $C_{1'}$ in pyrimidine and C_8 and $C_{1'}$ in purine residues were obtained at 298 K. The relaxation data were analyzed by the model-free formalism to yield dynamic information on timescales of pico-, nano- and milli-seconds. An axially symmetric diffusion tensor with an overall rotational correlation time τ_c of 2.31 ± 0.13 ns and an axial ratio of 1.35 ± 0.02 were determined. Both findings are in agreement with hydrodynamic calculations. For the nucleobase carbons, the validity of different reported ^{13}C chemical shift anisotropy values (Stueber, D. and Grant, D. M., 2002 *J. Am. Chem. Soc.* **124**, 10539–10551; Fiala et al., 2000 *J. Biomol. NMR* **16**, 291–302; Sitkoff, D. and Case, D. A., 1998 *Prog. NMR Spectroscopy* **32**, 165–190) is discussed. The resulting dynamics are in agreement with the structural features of the cUUCGg motif in that all residues are mostly rigid ($0.82 < S^2 < 0.96$) in both the nucleobase and the ribose moiety except for the nucleobase of U7, which is protruding into solution ($S^2 = 0.76$). In general, ribose mobility follows nucleobase dynamics, but is less pronounced. Nucleobase dynamics resulting from the analysis of ^{13}C relaxation rates were found to be in agreement with ^{15}N relaxation data derived dynamic information (Akke et al., 1997 *RNA* **3**, 702–709).

Introduction

In proteins, residue specific dynamic information is routinely extracted from ^{15}N NMR relaxation parameters. Relaxation of the backbone amide nitrogens can be described to a good approximation in the context of an isolated I–S spin system, with S signifying the nitrogen and I the directly attached proton. A number of formalisms have been derived for the interpretation of autocorrelated relaxation parameters relying on I–S spin system type relaxation behavior (Lipari and Szabo, 1982a; Peng and Wagner, 1992; Ishima and Nagayama, 1995; Farrow et al., 1995). Using these formalisms, amide nitrogen relaxation can be translated into dynamic parameters, providing one dynamic probe for each residue in a protein.

In contrast, in oligonucleotides, due to imino hydrogen exchange with water, NH moieties are only observed for nucleotides involved in hydrogen bonding. Typically, only one NH moiety is present in each base-pair, while dynamic residues or non-canonical regions such as loops or bulges cannot be investigated by ^{15}N relaxation. In addition, even if a NH moiety can be detected, ^{15}N

*To whom correspondence should be addressed. E-mail: schwalbe@nmr.uni-frankfurt.de

relaxation can only report on nucleobase dynamics, whereas no dynamic information on either the ribose ring or the backbone can be obtained.

In contrast, ^{13}C relaxation can in principle report on the dynamics of both the ribose and the nucleobase moiety in all nucleotides. However, unless labeling schemes at specific positions are employed, only C_8 and C_2 in adenine and C_8 in guanine are located within isolated CH groups. For the remaining ^{13}C sites, relaxation does not follow I–S spin system relaxation. Therefore, the effect of neighboring ^{13}C nuclei has to be considered, both in the experimental schemes and in the dynamic analysis. So far, efforts to obtain quantitative dynamic information on oligonucleotides from ^{13}C relaxation data have been aimed at ensuring an isolated I–S spin system type relaxation behavior. This comprises of selective labeling of specific ^{13}C sites (Olsen et al., 1982; Schmidt et al., 1983, 1987; Williamson and Boxer, 1989; Gaudin et al., 1995), uniform partial ^{13}C enrichment (Kojima et al., 1998; Boisbouvier et al., 1999), measurements at ^{13}C natural abundance (Lane, 1991; Borer et al., 1994; Spielmann, 1998) or restriction of the dynamic analysis to the isolated C_2 and C_8 spins in uniformly labeled samples (Hall and Tang, 1998). However, for small systems with rotational correlation times of up to 4 ns, the C–C dipolar contribution is small compared to the C–H contribution, and the various C–H moieties in a uniformly labeled compound can, to a good approximation, be treated as I–S spin systems (Paquet et al., 1996; Boisbouvier et al., 2003).

Apart from the deviation from I–S spin system type relaxation, the paucity of information on the ^{13}C chemical shift anisotropy (CSA) in oligonucleotides constitutes an obstacle in the routine dynamic interpretation of ^{13}C spin relaxation, in which an axially symmetric CSA with its unique principal axis oriented collinear with the I–S bond vector is assumed. However, both for the ribose and the nucleobase carbons, fully anisotropic and non-collinear chemical shift tensors have been consistently reported (Dajaegere and Case, 1998; Boisbouvier et al., 2000; Fiala et al., 2000). In the case of the ribose carbons, the CSA amounts only to around 30–60 ppm and the contribution of the CSA relaxation mechanism is therefore minor compared to the C–H dipolar mechanism even at high magnetic fields. Thus, the error introduced into the model-free analysis is small and can be neglected (Boisbouvier et al., 2003). In contrast, in the nucleobases the carbon CSA is much larger, indicating that CSA relaxation cannot be neglected for the aromatic carbons. So far, only one quantitative dynamic study on RNA has been reported on C_2 and C_8 spins in adenine and guanine, which utilized the CSA-value obtained for C_6 in thymine (Williamson and Boxer, 1989) for both spins. However, recently reported nucleotide CS-tensors obtained from DFT calculations (Fiala et al., 2000) and from solid state investigations on mononucleoside powders (Stueber and Grant, 2002) report significant differences between the different aromatic carbon sites.

In this report, the dynamic properties of C_6 and C_8 in the nucleobase moieties of pyrimidine and purine residues, respectively, and of $C_{1'}$ in the ribose moiety (Figure 1a) of all residues of a uniformly $^{13}C/^{15}N$ labeled 14-nt cUUCGg hairpin (Figure 1b) have been investigated. $C_{1'}$ as well as C_6 possess only one adjacent carbon spin, from which they are sufficiently well resolved in order to allow for a selective excitation as required for C–C decoupling in general as well as in $R_{1\rho}$-experiments. In addition, due to their similar resonance

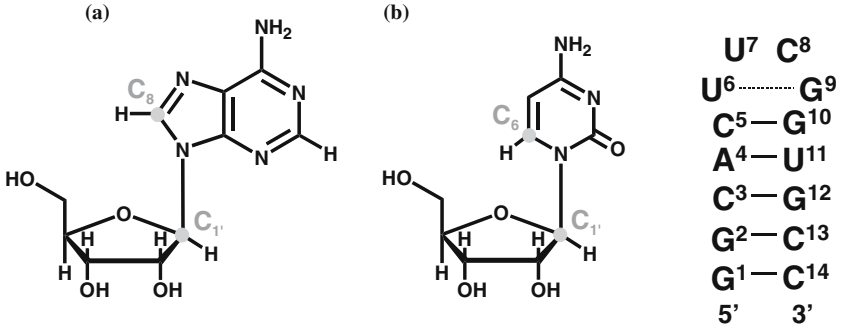

Figure 1. (a) Investigated ^{13}C sites (grey dots) in purines and pyrimidines and (b) secondary structure of the 14-nt RNA.

frequencies, C_6 and C_8 can be addressed within the same experimental scheme.

Theoretical section

Relaxation of a ^{13}C spin is dominated by the dipolar interaction with its directly attached proton and by its own chemical shift anisotropy (CSA). The dependence of the spin-lattice (R_1), the spin–spin (R_2) autocorrelated relaxation rate and the ^{13}C-{^1H} steady-state NOE for an isolated C–H spin system on the two relaxation mechanisms have been developed (Abragam, 1961) and can be found e.g. in Akke et al. (1997).

Autocorrelated relaxation parameters can be interpreted in the context of the model-free approach (Lipari and Szabo, 1982a, b), which results in the generalized order parameter S^2 as a measure for the spatial restriction of the internal motion and an effective correlation time τ_e defining the timescale of internal motion. The formulae for isotropic and anisotropic diffusion are given in Akke et al. (1997).

Although in the model-free analysis no specific motional models are assumed a priori, the order parameter can be interpreted within the context of specific models for the underlying dynamic processes. Thus, in cases of independent motions of either the base or the ribose moiety, the S^2 parameter associated with a C–H vector can be translated into the amplitude of the motion around the glycosidic torsion angle χ through application of the Gaussian axial fluctuation (GAF) model (Brüschweiler and Wright, 1994). The GAF describes a Gaussian distribution of bond vectors on the surface of a cone. The S^2 parameter and the angle β between the C–H vector and the cone-axis define the amplitude of axial fluctuation:

$$S^2 = 1 - 3\sin^2\beta \times \left[\cos^2\beta\left(1 - e^{-\sigma_\chi^2}\right) + \frac{1}{4}\sin^2\beta\left(1 - e^{-4\sigma_\chi^2}\right)\right] \quad (1)$$

In Equation 1, β is the angle between the C–H vector and N_1/N_9–$C_{1'}$, the director axis of the cone, and σ_χ^2 is the standard deviation of the fluctuation in the azimuthal angle, corresponding to the fluctuation in χ.

Experimental section

Sample preparation

The uniformly $^{13}C/^{15}N$ labeled 14-nt RNA (5′-PO_4^-GGCAC**UUCG**GUGCC-3′; bold residues constitute the loop) was purchased from Silantes GmbH (Munich, Germany). The concentration of the NMR sample was 0.7 mM in 20 mM KH_2PO_4/K_2HPO_4, pH 6.4, 0.4 mM EDTA and 10% v/v D_2O.

NMR spectroscopy

All NMR experiments were carried out on a 600 MHz Bruker spectrometer equipped with a 5 mm $^1H\{^{13}C/^{15}N\}$ Z-Grad TXI probe. ^{15}N R_1, $R_{1\rho}$ and ^{15}N-{^1H} steady-state NOE data were obtained from the pulse sequences hsqct1etf3gpsi3d, hsqctretf3gpsi3d.2 and invnoef3gpsi comprised in the Bruker pulse sequence library (Kay et al., 1992; Farrow et al., 1994; Mulder et al., 1998; Korzhnev et al., 2002). ^{13}C R_1, $R_{1\rho}$ and ^{13}C-{^1H} steady-state NOE data were obtained using ^{13}C modifications of the pulse sequences used for the ^{15}N relaxation measurements. The carrier frequency was set to 139 ppm for the aromatic carbons and 89 ppm for $C_{1'}$. The spectral width was 5 ppm for the base and 6 ppm for the ribose moiety. About 64–100 complex points were acquired in the indirect dimension. Off-resonant carbon Q3 pulses (512 μs) were applied during carbon evolution with an offset of −7500 Hz or −5000 Hz in order to suppress the $^1J(C_5, C_6)$ and $^1J(C_{1'}, C_{2'})$ coupling, respectively. During the chemical shift evolution periods, long range C_6, C_4 and C_8, C_4 couplings were assumed to be negligible. Relaxation delays of 2 s were applied between the scans for the R_1 and $R_{1\rho}$ measurements, 5 s were used for the NOE. R_1 and $R_{1\rho}$ data were obtained with 8, the NOE with 16 scans for each t_1-increment. R_1- and$R_{1\rho}$-subspectra with varying relaxation delays were acquired in one interleaved pseudo-3D experiment. The NOE experiments were also recorded interleaved, with alternating proton-presaturated and non-presaturated spectra. While in the latter case, a relaxation delay of 5 s was used, proton-presaturation was applied for 3 s subsequent to a 2 s relaxation delay in the presaturated spectra. The interleaved spectra were separated by a Bruker standard macro.

For the acquisition of R_1 relaxation rates, the relaxation delay τ_M was set to 10, 50, 100, 200, 400, 700 ms, 1 and 1.5 s. Spectra with $\tau_M = 50$ and 400 ms were recorded twice for error determination.

$R_{1\rho}$ rates were acquired as described (Mulder et al., 1998; Korzhnev et al., 2002). Random length proton decoupling pulses were applied during the carbon spin-lock period (option **d** in Korzhnev et al., (2002)). Adiabatic Mulder pulses (Mulder et al., 1998) were used to rotate the carbon magnetization into the transversal plane. A spin-lock field of 3.6 kHz with an offset of 2000 Hz was applied for the variable relaxation delay ($\tau_M = 12$, 24, 36, 48, 64, 80, 104, 128 ms). Duplicate measurements were carried out for $\tau_M = 24$ and 80 ms.

Data analysis

The data were processed on a Silicon Graphics computer (Origin2000) using Bruker NMRSuite (XwinNMR 3.5) programs and analyzed in Felix2000 (msi). R_1 and $R_{1\rho}$ relaxation decays were fitted from peak heights to monoexponential two-parameter functions using macros provided by Palmer and co-workers (Stone et al., 1992).

The measured $R_{1\rho}^{meas}$ rates contain spin-lock offset and spin-lock power dependent contributions of R_1 and R_2. From $R_{1\rho}^{meas}$ and R_1, R_2 can be extracted following Equation 2.

$$R_2 = \frac{R_{1\rho}^{meas} - R_1 \cos^2\theta}{\sin^2\theta} \tag{2}$$

In this, θ is the angle of the effective spin-lock field with the B_0 field for each nucleus defined according to:

$$\theta = \tan^{-1}\left(\frac{\nu}{\Omega}\right) \tag{3}$$

in which ν is the spin-lock field strength and Ψ is the resonance offset from the spin-lock carrier, both in Hertz.

In uniformly isotopically enriched samples, it is important to ensure that homonuclear Hartmann–Hahn magnetization transfer to the adjacent as well as remote carbon spin is minimized during the spin-lock period of the $R_{1\rho}$ measurement. The maximum amount of net Hartmann–Hahn magnetization transfer between two spins 1 and 2 is given by Equation 4 (Bax and Davis, 1985):

$$R_{1,2}^{max} = \left[J_{1,2}{}^2\{1+\cos(\theta_1-\theta_2)\}^2\right] \Big/ \times \left[4\left(\nu_{1,eff}-\nu_{2,eff}\right)^2 + J_{1,2}{}^2\{1+\cos(\theta_1-\theta_2)\}^2\right] \tag{4}$$

In this, $J_{1,2}$ is the coupling constants between spin 1 and 2, θ_i is the spin-lock angle of spin i as defined by Equation 3 and $\nu_{i,eff}$ is the effective field-strength experienced by nucleus i given by $(\nu^2 + \Omega_i^2)^{1/2}$. As apparent from Equation 4, the Hartmann–Hahn transfer is most efficient between spins with similar effective field strengths and high coupling constants. In the 14-nt RNA, the highest maximum Hartmann–Hahn magnetization transfer is about 1.5‰ between $C_{1'}$ and $C_{2'}$ of residue C8, as calculated from a coupling constant of 42 Hz, a spin-lock field-strength of 3600 Hz and a difference in effective field strengths of 1710 Hz. For long-range carbon–carbon couplings between C_8 and C_4, C_5 or C_6 in purines or C_6 and C_4 or C_2 in pyrimidines with coupling constants of around 4–12 Hz (Wijmenga and van Buuren, 1998), the transfers are about one or two orders of magnitude less efficient than the transfer between adjacent spin pairs ($C_{1'}$, $C_{2'}$ and C_6, C_5, respectively). Therefore, the $R_{1\rho}$ rates obtained in here can be considered free of any Hartmann–Hahn contribution.

The model-free analysis of the relaxation parameters has been carried out using the program *Modelfree 4.15* by Palmer and co-workers (Mandel et al., 1995). Vibrationally averaged effective bond lengths were used for the N–H (1.04 Å; Case, 1999) as well as for the C_6–H_6, C_8–H_8 (both 1.08 Å) and the $C_{1'}$–$H_{1'}$(1.09 Å) bond. Model selection followed the procedure recommended in Mandel et al., (1995) and is described in detail in annex I in the Supporting Information. Diffusion parameter optimization was carried out during an initial grid search in *Modelfree*. The diffusion parameters obtained from *Modelfree* were compared to hydrodynamic calculations performed with the program *hydronmr 5a* (Garcia de la Torre et al., 2000).

Results and discussion

R_1, R_2 and NOE data for $C_{1'}$, C_6 and C_8 of the 14-nt hairpin at 298 K are shown in Figure 2a and summarized in Table S1 in the Supporting Information. Representative R_1 and $R_{1\rho}$ relaxation

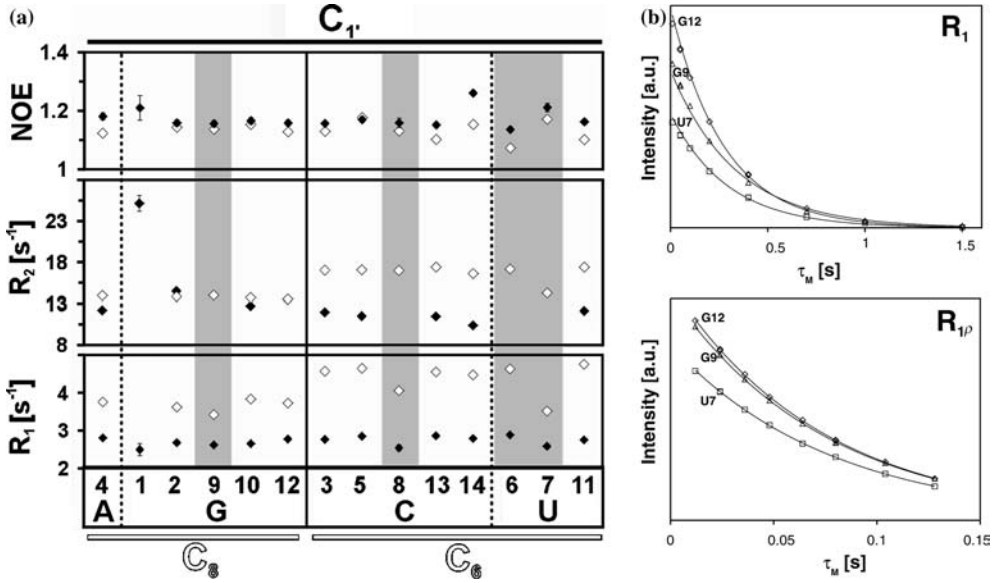

Figure 2. (a) Measured and ^{13}C-{^{1}H} NOEs, R_2 and R_1 of $C_{1'}$ (full diamonds) and C_6/C_8 (open diamonds) of the 14-nt RNA at 298 K sorted by base type. Loop residues are shaded in grey. (b) R_1 (top) and $R_{1\rho}$ (bottom) relaxation decay curves of C_6 and C_8 for residues U7, G9 and G12. Peak heights (in arbitrary units) are plotted against the relaxation delay τ_M. The curves represent monoexponential two-parameter fits. Duplicate data sets acquired in order to obtain errors for the peak intensities are included in the graphs.

decay curves (Figure 2b) exhibit a monoexponential behavior for C_8 as well as C_6 even at longer relaxation delays indicating that contributions from C–C cross relaxation remain negligible.

The carbon CSA

Three studies on ^{13}C CS-tensors in nucleotide base moieties have been reported to date, one in which the CS-tensor has been determined from DFT calculations based on chemical shift components measured in mononucleosides by solid state NMR measurements (Stueber and Grant, 2002) and two exclusively relying on DFT calculations (Sitkoff and Case, 1998; Fiala et al., 2000). In all three studies, the CS-tensors of C_6 and C_8 are oriented with their most shielded component orthogonal to the base plane. The two remaining components are located within the base plane, with the most deshielded component tilted away from the C–H internuclear vector by around 30°. The anisotropies of the three sets of C_6 and C_8 CS-tensors are summarized in Table 1.

For all three sets of CSAs, the C_6 values for cytidine and uridine and the C_8 values for adenine and guanine are very similar. Furthermore, the values of C_6 are about 45–65 ppm larger than the ones of C_8. The R_1 and R_2 relaxation rates observed in the 14-nt RNA are on average about 20% larger for C_6 than for C_8 (Figure 2). A difference of 45 ppm accounts for around 15%, a difference of 65 ppm for almost 30% deviation in the relaxation rates, indicating that the observed differences between C_6 and C_8 relaxation rates can be fully explained by the reported CSA values.

Table 1. CSA values for C_6 and C_8 reported by Fiala et al. (2000), Stueber and Grant (2002) and Sitkoff and Case (1998)

		CSA [ppm]		
		Fiala et al.	Stueber et al.	Sikoff et al.
C_8	Adenine	−123	−134	−114
	Guanine	−119	−134	−113
C_6	Cytidine	−184	−179	−157
	Uridine	−184	–	−167

For the C_8 sites of the purine residues, significantly lower overall residual errors ($\chi^2 = 16.1$) are achieved in the model-free analysis with the CSA from the solid-state NMR investigation (Stueber and Grant, 2002) than when the CSAs of either DFT-study are used ($\chi^2 = 23.0$ (Fiala et al., 2000) and $\chi^2 = 27.3$ (Sitkoff and Case, 1998)). The C_8 CSA from the solid-state NMR investigation is

−134 ppm for both adenine and guanine and around 10–20 ppm larger than the CSAs from the two DFT-studies, respectively. Also for C_6, higher CSA values result in a better overall fit in the model-free analysis. For uridine, no CS-tensor is available from the solid-state analysis. However, if the C_6 CSA of cytidine is used, the overall χ^2-value for the CSA values reported by Fiala et al. (2000) and the solid-state NMR analysis are very similar and significantly lower than for the CSAs from Sittkoff and Case (1998). While the former two C_6 CSAs are very similar (−184 and −179 ppm, respectively), the values reported by Sitkoff and Case (1998) are again significantly smaller (−157 ppm for cytidine, −167 ppm for uridine). Since the CSA values from the solid-state NMR analysis are in general in better agreement with the data, they have been used for both C_6 and C_8 in the following.

In the case of $C_{1'}$, different CSA values have been reported and a dependence on ribose puckering has been determined. While 30 ppm (Dajaegere and Case, 1998) or 45 ppm (Fiala et al., 2000) have been determined for the $C_{1'}$-sites in the $C_{3'}$-*endo* conformation, 60 ppm have been reported for $C_{2'}$-*endo* (Dajaegere and Case, 1998). In the solid-state NMR investigation, CSA values between 29 and 44 ppm have been obtained (Stueber and Grant, 2002). The smaller CSA of the aliphatic as compared to the aromatic carbon is reflected in the smaller R_1 and R_2 values of $C_{1'}$ compared to C_6 and C_8 (Figure 2b).

Although, due to the lower CSA-values, deviations from the actual values have a smaller effect on the $C_{1'}$ compared to the C_6 and C_8 relaxation data analysis, the CSA for this site has been optimized as well. An overall improvement is achieved with CSA-values of 45 ppm as compared to 30 ppm (χ^2 of 35.9 compared to 49.5). In contrast to a number of other residues, U7 and C8, which are in $C_{2'}$-*endo* conformation, do only show very small improvements when fitted with a CSA of 60 ppm as compared to 30 ppm (χ^2 of 0.67 compared to 1.15). Therefore, a CSA of 45 ppm has been used for all residues irrespective of their ribose pucker.

The C–H distance

Commonly used C–H bond lengths are 1.09 and 1.08 Å for $C_{1'}$ and C_6/C_8 (Bryce et al., 2004), respectively. However, more detailed studies carried out by (Case, personal communication) indicate, that zero-point motion averaged C–H bond length are actually about 0.02–0.03 Å longer (1.118 Å for longer by $C_{1'}$, 1.100 Å for C_6 and 1.103 Å for C_8). Incorporation of these bond lengths into the dynamic analysis yields order parameters ranging from 0.826 to 0.974 for $C_{1'}$ and from 0.759 to 0.979 for C_6 and C_8, respectively, for the shorter bond lengths. Higher S^2-values between 0.863 and 1.106 and between 0.813 and 1.052 are obtained for $C_{1'}$ and C_6/C_8, respectively, for the fully zero point motion corrected dipole lengths. By definition, the order parameters cannot exceed unity. While in case of the aromatic carbons, it could be argued that their CSA might be underestimated, for $C_{1'}$ the CSA relaxation mechanism constitutes only a minor contribution to overall relaxation and therefore this site represents a better probe for the relevance of the different bond lengths. Therefore, dipole lengths of 1.09 and 1.08 Å have been used in here for $C_{1'}$ and C_6/C_8, respectively. From this analysis, the reason for the inconsistency between the fully zero-point averaged bond lengths remains unclear.

The diffusion model

Hydrodynamics calculations using the program *hydronmr* (Fernandes et al., 2002) indicate that an axially symmetric diffusion model is sufficient to describe the 14-nt RNA (moments of inertia 1.00, 0.98 and 0.50). Therefore, diffusion model selection comprised the comparison between an isotropic and an axially symmetric model using the program *Modelfree* (Mandel et al., 1995). Since the structure of the investigated 14-nt RNA has not been solved so far, C–H vector orientations for calculation of the axially symmetric diffusion tensor were obtained from a 14-nt RNA molecule with the loop residues and the loop closing basepair from the X-ray structure (Ennifar et al., 2000) attached to a canonic A form stem of appropriate sequence. Separate fits were carried out for the nucleobase and the ribose carbon relaxation data. Due to their increased mobility, the $C_{1'}$ data of the two terminal residues as well as the C_6 data of U7 were only included into the fitting procedure after diffusion model optimization.

An axially symmetric diffusion model consistently yielded smaller residual errors than an

isotropic one. An overall rotational correlation time of 2.44 ns and a diffusion anisotropy of 1.32 were determined from the analysis of the $C_{1'}$ data. For the C_6/C_8 data, a similar diffusion anisotropy ($D_{\parallel/\perp} = 1.37$) but a slightly lower correlation time ($\tau_c = 2.18$ ns) were obtained. These values are in good agreement with hydrodynamic calculations using the program *hydronmr* ($\tau_c = 2.47$ ns; $D_{\parallel/\perp} = 1.40$). For both the $C_{1'}$ and the C_6/C_8 data, the unique principal axis of the diffusion tensor is tilted 20–30° from the one of the hydrodynamic tensor.

The data is furthermore consistent with an earlier dynamic study carried out on the 14-nt RNA at 278 K based on ^{15}N relaxation rates, in which an anisotropy of 1.34 has been reported (Akke et al., 1997). However, in order to compare the ^{13}C and ^{15}N data at the same temperature, the respective relaxation data (Table S2, Supplementary Material) have been obtained for the N_1 and N_3 spins of residues G2, G9, G10, U11 and G12 at 298 K. These data resulted in a correlation time of 2.21 ns and an anisotropy of 1.33.

Model-free analysis

The results of the model-free analysis of the ^{13}C relaxation data are summarized in Table 2. Model-free parameters are given for an isotropic as well as for an axially symmetric diffusion model. In the following, C_6 and C_8 will be considered reporters on the flexibility of the entire nucleobase moiety, while $C_{1'}$ dynamics will be treated as reflecting the mobility of the whole ribose moiety. It has to be kept in mind, however, that any given I–S vector is sensitive to a different degree to different motions depending on their relative direction, signifying that one vector alone can never supply complete motional information on any system.

For a number of residues, the isotropic diffusion model leads to more complicated motional models than the axially symmetric one. Thus, additional chemical exchange terms are required for the ribose moieties of A4, G9, G10 and U11 and for the base moiety of C8, whereas these residues can be fitted to the simplest motional model ($\tau_e \sim 0$; $S_f^2 = 1$; $R_{ed} = 0$) when anisotropic diffusion is considered. Also for the base moiety of U7, an additional R_{ex} term is required, while this moiety shows only fast time-scale internal motion ($\tau_e > 0$) with the axially symmetric diffusion model. The ribose moiety of this residue only exhibits slow exchange in the more complicated diffusion model, whereas an isotropic model requires an additional fast exchange term. In addition, for a number of residues, which exhibit slow exchange or picosecond internal motion, the respective contributions are higher in the isotropic as compared to the anisotropic case. In all these cases, the neglect of anisotropic diffusion is compensated by additional motional terms. On the contrary, the bases of C5 and C14 reveal a more complicated motional behavior, when an axially symmetric diffusion model is employed. In this case, both moieties require R_{ex}-terms in addition to picosecond internal motion ($\tau_e > 0$). In conclusion, this indicates that even in case of the small anisotropy of the 14-nt RNA, the neglect of its anisotropy can lead to significant misinterpretations of the relaxation data. Therefore, only the axially symmetric diffusion model will be considered in the following:

The relaxation parameters of most of the sites can be fitted to the simplest motional model. While the 5′-terminal G1 shows a large R_{ex} contribution only in its ribose moiety, the 3′-terminal C14 exhibits a millisecond chemical exchange term and picosecond motions in its base moiety as well as picosecond motions on a slower time-scale and larger amplitude in its ribose moiety. This signifies that the residues in the terminal base pair are moving independently from each other, with the 3′-terminus exhibiting more extensive motion than the 5′-terminus. In contrast, the base moieties of the non-terminal residues are in general more flexible than the respective ribose moieties. Thus, slower time scale motions are observed for the base moieties of C5 and U7 ($\tau_e > 0$), while their ribose moieties exhibit faster dynamics ($\tau_e \sim 0$). A number of ribose (G2, U7, C8, G12) as well as base (G2, C5, G9) moieties exhibit chemical exchange contributions in the range of 1–4 s^{-1}.

S^2-values for the ribose and the nucleobase moiety are shown in Figure 3 for an isotropic (open diamonds) as well as an axially symmetric diffusion model (grey diamonds). As expected, the introduction of additional motional terms due to the disregard of anisotropic overall motion results in an overestimation of the extent of internal motion. This is most prominent for the ribose moieties of G1, G2, G9, G10, C8 and U7 and the

Table 2. Results of the model-free analysis of the 14-nt RNA. The results employing an axially symmetric model are shown in bold; the ones using an isotropic diffusion model are given in italics. C–H distances of 1.09 Å and 1.08 Å have been used for C_6/C_8 and $C_{1'}$, respectively. The CSA values were −134 and −179 ppm taken for C_8 and C_6 (Stueber and Grant, 2002), a CSA of 45 ppm was used for $C_{1'}$ (Fiala et al., 2000)

	C_6/C_8			$C_{1'}$			
	S_s^2	τ_e [ps]	R_{ex} [s^{-1}]	S_s^2	S_f^2	τ_e [ps]	R_{ex} [s^{-1}]
G1	*0.893* ± 0.053			*0.907* ± 0.058			*13.10* ± 1.24
	0.886 ± 0.067			*0.835* ± 0.054			*14.99* ± 1.17
G2	*0.884* ± 0.010		*0.98* ± 0.19	*0.958* ± 0.014			*1.95* ± 0.21
	0.878 ± 0.010		*1.20* ± 0.19	*0.896* ± 0.013			*3.59* ± 0.19
C3	*0.959* ± 0.009			*0.951* ± 0.004			
	0.961 ± 0.005			*0.963* ± 0.012			
A4	*0.911* ± 0.008			*0.974* ± 0.005			
	0.912 ± 0.005			*0.939* ± 0.014			*0.76* ± 0.18
C5	*0.909* ± 0.006	*70.96* ± 8.40	*1.04* ± 0.17	*0.947* ± 0.005			
	0.933 ± 0.005	*121.59* ± 17.56		*0.946* ± 0.005			
U6	*0.952* ± 0.019			*0.932* ± 0.018			
	0.953 ± 0.018			*0.936* ± 0.018			
U7	*0.759* ± 0.005	*18.01* ± 1.42		*0.918* ± 0.029			*2.52* ± 0.46
	0.706 ± 0.006	*13.38* ± 1.15	*2.18* ± 0.18	*0.848* ± 0.029		*15.74* ± 9.62	*4.05* ± 0.44
C8	*0.901* ± 0.009			*0.902* ± 0.029			*3.82* ± 0.42
	0.845 ± 0.005		*2.37* ± 0.16	*0.850* ± 0.027			*5.18* ± 0.38
G9	*0.819* ± 0.005		*2.15* ± 0.12	*0.943* ± 0.005			
	0.830 ± 0.004		*1.82* ± 0.10	*0.877* ± 0.014			*1.68* ± 0.18
G10	*0.908* ± 0.003			*0.956* ± 0.007			
	0.909 ± 0.011			*0.888* ± 0.013			*1.91* ± 0.18
U11	*0.979* ± 0.012			*0.960* ± 0.004			
	0.984 ± 0.008			*0.920* ± 0.011			*0.92* ± 0.15
G12	*0.868* ± 0.011			*0.941* ± 0.013			*1.82* ± 0.17
	0.866 ± 0.016			*0.928* ± 0.012			*2.18* ± 0.17
C13	*0.959* ± 0.009			*0.940* ± 0.007			
	0.960 ± 0.012			*0.946* ± 0.007			
C14	*0.909* ± 0.006	*33.35* ± 6.79	*0.43* ± 0.16	*0.907* ± 0.013	*0.910* ± 0.007	*389.99* ± 81.71	
	0.919 ± 0.005	*38.08* ± 6.63		*0.902* ± 0.013	*0.911* ± 0.007	*412.14* ± 78.92	
	τ_c = *2.18* ns; $D_{\parallel/\perp}$ = *1.37*			τ_c = *2.44* ns; $D_{\parallel/\perp}$ = *1.32*			
	τ_c = 2.17 ns			τ_c = 2.35 ns			

base moiety of C8. This emphasizes again the importance of including diffusion anisotropy even for molecules with small diffusion anisotropies.

For the axially symmetric diffusion model, the following conclusions can be drawn about the dynamics of the 14-nt RNA:

Order parameters range from 0.826 to 0.974 for the ribose and from 0.759 to 0.979 for the nucleobase moiety. Average S^2-values for $C_{1'}$, C_6 and C_8 of the non-terminal stem-residues (residues 2–5 and 10–13) are 0.953 ± 0.010, 0.952 ± 0.026 and 0.895 ± 0.018, respectively. Average order parameters for purine residues are about 0.06 or around 20% lower than for pyrimidines, indicating that the former are more flexible. However, the observed difference in average order parameters could also be due to the deviations of the reported C_6 or C_8 CSAs from the actual values. Either the C_8 CSA is overestimated or the C_6 CSA underestimated. Another potential source for the observed difference in the S^2-values could be found in differences in C–H bond vector lengths.

The order parameters are depicted in the context of the structure of the 14-nt RNA in

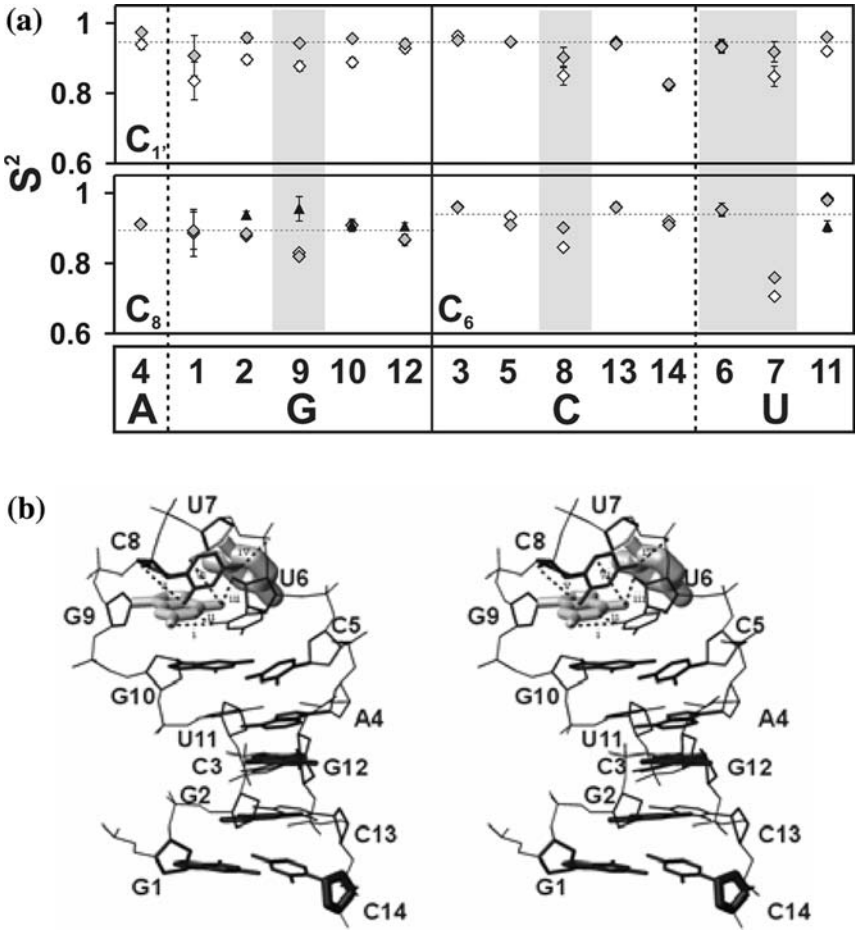

Figure 3. (a) Order parameters for $C_{1'}$ (top) and C_6/C_8 (bottom) sorted by base type. Fits to an isotropic diffusion model are shown as open diamonds; fits to an axially symmetric diffusion model are shown as grey filled diamonds. Horizontal dashed lines indicate the average S^2 of the respective stem residues. ^{15}N relaxation data derived order parameters with an axially symmetric diffusion model are shown as black triangles. The data have been obtained with N–H distances of 1.04 Å and N_1 and N_3 CSAs of −130 and −100 ppm, respectively. (b) Stereo view of the 14-nt RNA with the S^2-values of $C_{1'}$ and C_6/C_8 coded into bond thickness of the ribose and the base moiety, respectively. In order to stress the differences in order parameters, bond thickness is proportional to the inverse ninth power of S^2. The hydrogen bond interactions stabilizing the loop-structure are: (i) $G9(N_2)$–$U6(O_2)$; (ii) $G9(N_1)$–$U6(O_2)$; (iii) $U6(O_{2'})$–$G9(O_6)$; (iv) $C8(N_4)$–$U7(PO^{proR})$; (v) $C8(O_{2'})$–$C8(O_2)$; (**vi**) $U7(O_{2'})$–$G9(O_6)$.

Figure 4b. Apart from the 3′-terminal ribose and the nucleobase moiety of U7, all base as well as ribose moieties are more or less rigid. While the ribose moiety of C14 at the 3′-terminus exhibits considerably increased flexibility compared to the stem residues, its nucleobase moiety is only slightly more flexible than average. This indicates that the base moiety of this residue is involved in some stabilizing interaction like base stacking, while its ribose moiety is less motionally restricted. For the 5′-terminal G1, errors of the model-free analysis are high due to weak $C_{1'}$ and C_8 resonances. However, also for this residue, ribose flexibility seems to exceed nucleobase dynamics.

While the terminal base-pair shows increased flexibility, already the second stem base-pair (G2–C13) exhibits average stem mobility in both moieties, indicating that any terminal effects on the flexibility are restricted to the closing base-pair. The fourth base pair (A4–U11) constitutes the most rigid one, although it is an A–U base pair. The loop closing base pair (C5–G10) is slightly more flexible, with all moieties being rigid except for the base of C5, which is slightly less stable.

In the loop, only the ribose moiety of G9 and both moieties of U6 are as rigid as the stem residues. Whereas the nucleobase moieties of C8 and G9 exhibit only slightly increased flexibility, U7 is significantly more flexible ($S^2 = 0.706$). Of the ribose moieties, only U7 and to a slightly higher extent C8 show increased dynamics.

Also shown in Figure 4a are the order parameters obtained from the ^{15}N data at 298 K fitted to an axially symmetric diffusion model (black triangles). All residues can be fitted to the most simple motional model. Order parameters range from 0.905 to 0.955. An excellent agreement between the ^{13}C and the ^{15}N data is observed for G10 and G12, and the order parameters for G2 match as well although the agreement is slightly worse. However, significant differences are found for G9 and U11. For the latter, it has to be noted that only this one pyrimidine residue could be investigated by ^{15}N relaxation analysis. Thus, the origin between the two relaxation analyses is difficult to interpret in this case. The most evident explanation is, however, that the differences result from systematic errors arising from the choice in bond length or CSA for either or both sets of relaxation data. Considering the observed differences in ^{13}C purine and pyrimidine $C^{13}S^2$-values, which can most likely be also attributed to deviations of the employed from the actual CSAs, it can be speculated that the C_6 CSA is in fact larger than assumed. An increased C_6 CSA of about 20 ppm could decrease pyrimidine order parameters by 20% to the level of both C_8 and ^{15}N S^2-values.

The largest differences in the dynamic interpretation of ^{13}C and ^{15}N relaxation data are observed for G9. While the nucleobase of this residue appears even slightly more flexible than the stem residues in the ^{13}C relaxation data analysis, it seems to be the most rigid moiety in the 14-nt RNA from the ^{15}N analysis. This latter result is in agreement with the ^{15}N relaxation investigation reported earlier (Akke et al., 1997). In this case, the difference in order parameters between the two analyses is difficult to explain considering that a general agreement in ^{13}C and ^{15}N derived S^2-values is observed for three other guanine residues, indicating a consistency in the dipole lengths as well as CSAs. In the internally rigid base moiety, differences in the flexibility of the C–H and the N–H vectors have to be due to their different orientation, which renders them sensitive to different motions. The C_8–H_8 and the N_1–H_1 vector are not parallel in the base plane of guanine but form an angle of around 156°. Therefore, the orientation dependent motional sensitivity of the relaxation data could provide an explanation for the differences in the order parameters in this case. In addition, slightly different tensor orientations have been obtained for the ^{13}C as compared to the ^{15}N data, resulting in different angles of the respective vectors with the principal axis of the diffusion tensor. Another potential source for the observed discrepancy between the ^{13}C and the ^{15}N derived order parameters could be found in the conformational dependence of the CSAs. For G_9, which is in *syn* conformation around the glycosidic torsion angle, significant differences in Γ (H_8C_8, N_9) dipole–dipole, CSA cross-correlated relaxation rates compared to residues in *trans* conformation have been observed (Duchardt et al., in preparation). Since this cross-correlated relaxation rate probes a rigid unit, deviation in it have to arise from differences in the CSA of N_9 or/and C_8. This deviation of the CSAs for purines in the *syn* conformation could provide an explanation for the observed differences in ^{13}C and ^{15}N derived order parameters in this case.

Motional implications

The cUUCGg motif is a highly abundant RNA secondary structure motif of extraordinary thermodynamic stability ($T_m \sim 70$ °C; Varani, 1995). It has been extensively studied and characterized structurally both by NMR spectroscopy (Varani et al., 1991; Allain and Varani, 1995) and X-ray crystallography (Ennifar et al., 2000; Nissen et al., 2000; Wimberly et al., 2000). Its structural features (Figure 4b) comprise base-pairing of the two lower loop residues with the G at position four in *syn* conformation. This base-pair is stabilized by a bifurcated base-to-base as well as a base-to-ribose hydrogen bond. The actual loop is formed by the two apical residues, which adopt $C_{2'}$-*endo* ribose puckering and thereby extend the backbone across the strands. The second loop residue is free from any interaction with the other residues except for a hydrogen bond between its ribose and the nucleobase moiety at loop position four, which has been reported only for the X-ray structure (Ennifar et al., 2000). The nucleobase of the cytosine at loop

position three forms an interresidual hydrogen bond with the phosphodiester-backbone at position two and an intraresidual base-to-ribose hydrogen bond. In addition to hydrogen bonding, further stabilization is obtained from extensive base-stacking of loop residues three and one and the 5′-terminal partner of the closing base-pair.

Although the exact quantification of motional amplitudes based on model-free parameters is hampered by uncertainties regarding the C–H bond length as well as the carbon CSA, relative amplitudes can be assessed. In addition, dynamic information on both the ribose and the nucleobase moiety allow the deduction of qualitative information about the underlying motional processes. In the following, motional implications of the model-free parameters obtained on the cUUCGg motif will be discussed in more detail:

The nucleobase moiety of residue U7 is the most flexible site in the molecule. In addition, the base moiety of G9 exhibits increased dynamics but to a lesser extent. While the base moieties of these two residues are flexible, their ribose moieties do not exhibit increased dynamics. For U7, increased flexibility of the nucleobase is in agreement with the structure of the cUUCGg motif (Figure 3b), since the nucleobase of U7 is not involved in any stabilizing interaction. In contrast, the observed dynamics of the G9 nucleobase is surprising, since it is highly stabilized by three hydrogen bonds. Furthermore, for its base-pairing partner U6 no increased motions can be detected. Under the assumption that nucleobase flexibility monitored by the order parameters of C_6 and C_8 originate exclusively from independent base motions around the glycosidic torsion angle χ, S^2-values can be translated into a Gaussian distribution of motions around the $C_{1'}$–N_1 or $C_{1'}$–N_9 director axis modeled by the GAF-model (Equation 1; Brüschweiler and Wright, 1994). The decreased S^2 values for the nucleobases of U7 and G9 translate into χ angle fluctuation amplitudes of 23° and 16°, respectively. In contrast, the average stem fluctuation angles are $9° \pm 1$ for the pyrimidines and $12° \pm 1$ for the purines. This is in agreement with a higher degree of spatial restriction of the pyrimidines than the purines (Sänger, 1984). This signifies that the χ angle fluctuations are only slightly elevated for G9 as compared to the stem purines, indicating that the increase in flexibility as compared to the stem is small and could be displayed without structural disruptions. For U7, the base fluctuation amplitudes are more than two times as wide as for the stem pyrimidines. Given that the base of U7 is not involved in any stabilizing interactions but protrudes freely into solution, this degree of restriction is surprising. However, the rigidity of the U7 ribose moiety in combination with the steric hindrances originating from the surrounding loop structure might account for the observed motional restriction.

Apart from the U7 and G9 base moieties, both the base and the ribose moiety of residue C8 exhibit slightly increased flexibility. This residue is stabilized by a hydrogen bond to the phosphodiester backbone as well as base-stacking interactions with U6. In addition, the base and the ribose moiety are connected by an intraresidual hydrogen bond. This hydrogen bond could be kept, if the increased flexibility would be due to concerted motions of the whole residue. Localized backbone motions could result in concerted nucleobase and ribose motions of residue C8 as suggested by the similarity in the order parameters of the two moieties. This is consistent with an increased flexibility of the phosphorous of C8 compared to the other loop residues as apparent from R_1 relaxation measurements of ^{31}P in the backbone (Fürtig et al., in preparation).

For the stem residues, significantly higher nucleobase fluctuation amplitudes of 19–20° have been reported in the earlier ^{15}N relaxation study (Akke et al., 1997). In this case, order parameters ranged between 0.740 and 0.807, suggesting a much higher degree of overall flexibility. However, in this investigation, a shorter N–H dipole length, which was not corrected for zero-point motion, was used. This results in decreased order parameters and thus higher χ angle fluctuation amplitudes. Although absolute motional amplitudes might be slightly misjudged due to uncertainties in the C–H bond lengths as well as the CSA-values, a tentative interpretation of this result can be performed. A 9° or 12° fluctuation of the nucleobase around χ corresponds to a translatory motion of H_6 or H_8 of about ± 0.17 and ± 0.22 Å, respectively. For H_2 in adenosine, which is located at a larger distance in respect to the director axis, the motion is increased to ± 0.46 Å. These fluctuations represent the inherent limits of the precision to which an oligonucleotide structure can be determined at room temperature even in stably base-paired regions.

Conclusions

The aim of this report was to provide sensible probes for the residue specific dynamic investigation of RNA in general. In particular, these dynamic probes were used to study the dynamics of the abundant cUUCGg tetraloop motif at a high level of detail.

Due to the multitude of carbon spins within every RNA residue, ^{13}C NMR relaxation presents a versatile dynamic probe, in theory. In this report, the relaxation of C_6 in pyrimidines and C_8 in purines as well as $C_{1'}$ in all nucleotides has been investigated as dynamic reporters for the nucleobase and the ribose moiety, respectively. The quantitative dynamic interpretation of NMR relaxation parameters is complicated mainly by the uncertainties in the CSA and the C–H dipole lengths. In case of the $C_{1'}$ carbons, the CSA is small and possible errors due to conformational dependence of the CSA as observed for the $C_{2'}$-*endo* compared to $C_{3'}$-*endo* conformation do not incorporate notable errors in the model-free analysis. With a CSA of 45 ppm for all residues, which was shown to fit better than smaller values, satisfying fits and uniform order parameters could be obtained along the sequence.

For the aromatic carbons, which possess larger CSAs, relaxation data analysis depends more strongly on the incorporated CSA values. In here, it could be shown, that CSA values of −134 ppm for C_8 and −179 ppm for C_6 from a solid state NMR investigation on mononucleotides (Stueber and Grant, 2002) are the CSA-values reported in the literature most suited for oligonucleotides in solution. However, significantly lower order parameters for the purines as compared to the pyrimidines suggest that absolute as well as relative CSA values of C_6 and C_8 are still not optimal. Comparison to ^{15}N relaxation data indicates that the C_6 CSA might be by around 20 ppm larger than assumed. The dynamic analysis will therefore benefit from a residue specific determination of CS-tensors possibly directly on oligonucleotides and in solution. This could be achieved by measurement of the anisotropic chemical shift under weakly aligning conditions in combination with cross-correlated relaxation rates involving the CSA of interest. Such investigations would allow for the determination of possible conformational CS-tensor dependencies. This could help to solve local discrepancies in ^{13}C and ^{15}N derived order parameters as observed for the nucleobase moiety of residue G9 in the 14-nt RNA, which have been attributed to the dependence of the N_9 CSA on the conformation of the glycosidic torsion angle χ in here. Furthermore, in the model-free analysis an axially symmetric CS-tensor is assumed with its unique main component oriented along the I–S internuclear vector. From the available data (Fiala et al. 2000; Stueber and Grant, 2002), all of the ^{13}C tensors in nucleotides are, however, fully anisotropic. Thus, in order to improve the analysis, the anisotropy of these tensors has to be incorporated into the model-free analysis.

In order to optimize dipole lengths, non zero-point averaged and zero-point averaged bond lengths have been compared both for C–H and N–H vectors. For C–H vectors, fully zero-point motion averaged dipole vectors (Case, personal communication) examined in this report have resulted in order parameters significantly higher than 1. Therefore, non-averaged dipole lengths of 1.09 and 1.08 Å have been used both for $C_{1'}$ and C_6/C_8. It has to be noted, however, that for the analysis of ^{15}N relaxation data non-zero point averaged bond lengths of 1.02 Å result in significantly lower order parameters than the ones obtained from the ^{13}C relaxation analysis using non-averaged bond lengths. In contrast, zero-point averaged bond lengths of 1.04 Å (Case, personal communication) yield similar order parameters than the ones obtained from the ^{13}C relaxation analysis.

In here, average order parameters of 0.944 ± 0.012 for $C_{1'}$ and 0.938 ± 0.029 and 0.881 ± 0.029 for C_6 and C_8, respectively, have been observed. The similarity in order parameters between the ribose and the nucleobase moiety is in agreement with recent molecular dynamics simulations on RNA (Pan and MacKerell, 2003). Due to differences in the incorporated CSAs and bond lengths, a quantitative comparison to earlier studies is difficult. For instance, average stem S^2 values of 0.8 for C_2 and C_8 in purine bases have been reported at 298 K for the 16-nt iron responsive element RNA hairpin (Hall and Tang, 1998). However, considerably larger CSA values of −185 ppm and only slightly increased C–H distances of 1.09 Å have been used for the purine C_2 and C_8 sites. Slightly higher stem S^2 values of 0.6–0.9 have been determined for the adenine C_6/C_8 in the 30-nt TAR RNA at 298 K (King et al., 1995)

with a CSA of 180 ppm for both sites, while the dipole length is not mentioned in this case.

Apart from the consistency with earlier investigations on different RNA molecules, it could be demonstrated that the order parameters obtained from the ^{13}C sites in nucleobases are in general in good agreement with the ones from ^{15}N relaxation data acquired in here.

Optimized CSA values and bond lengths were used to investigate the dynamics of every ribose and nucleobase moiety of a 14-nt hairpin RNA containing the cUUCGg motif with $C_{1'}$ as the reporter for ribose and C_6/C_8 as a probe for the nucleobase moiety.

A comparison between different diffusion models demonstrates that the simplified model of isotropic diffusion may lead to a significant overestimation of local flexibility in some cases even for small RNA molecules like the 14-nt hairpin. This is in agreement with an earlier ^{15}N relaxation data investigation on proteins (Tjandra et al., 1995), where the relevance of a diffusion anisotropy of only 1.2 could be demonstrated in the case of human ubiquitin.

The comprehensive and exhaustive dynamic investigation of the 14-nt RNA cUUCGg tetraloop presented here indicates that the extraordinary thermodynamic stability of this RNA secondary structure motif is also reflected in its dynamic properties. Increased flexibility is localized and of small amplitude. Thus, all residues are rigid at room temperature except for the nucleobase of U7 and to a lesser extent the base moiety of G9 and the base as well as the ribose moiety of C8. These results are in general agreement with the structure of the cUUCGg tetraloop, in which all residues but the base moiety of U7 are involved in stabilizing interactions.

The increasing interest in RNA dynamics is demonstrated by the publication of two additional NMR relaxation investigations on the cUUCGg (Shajani and Varani, 2005; Vallurupalli and Kay, 2005) during the revision process of this manuscript. Vallurupalli and Kay studied the relaxation of C–D vectors in a partly deuterium enriched sample of the 14-nt RNA investigated in here. Although an intensive investigation was carried out, probing all C–D vectors in the ribose, and positions 5 and 6 in pyrimidines, the work was restricted to H–C–C–D and H–C–D sites and no information on purine base dynamics could be obtained. However, the dynamics of the remaining sites are in general in agreement with the results presented here in that the nucleobase of the second loop residue is the only flexible moiety in this molecule. The second study (Shajani and Varani, 2005) comprised the analysis of $C_{1'}$ and C_5, C_6 and C_8 relaxation of a larger RNA containing the cUUCGg motif. While ribose dynamics are similar to this report, base flexibilities differ. In this case, the G at position 4 is the most flexible loop residue and both uracil residues exhibit increased dynamics, whereas the C at position 3 is the only rigid loop residue. Unfortunately, the reasons for the deviation between this analysis and the one presented here cannot be assessed, since in the former report diffusion anisotropy has been neglected, very different C_8 and C_6 CSA values have been used and the incorporated C–H dipole lengths have not been stated.

Acknowledgements

The work was supported by the DFG (Sonderforschungsbereich 579), the state of Hesse, and the Fonds der Chemischen Industrie. We are grateful to David Case for the provision of dipole lengths used in this work. We wish to thank Jens Wöhnert, Hashim Al-Hashimi, Christian Richter and Emily Collins for fruitful discussions. E. D. is grateful to Jan Ferner for continuous stimulating discussions.

Electronic supplementary material is available at http://dx.doi.org/10.1007/s10858-005-0659-x

References

Abragam, A. (1961) *Principles of Nuclear Magnetism* Claredon Press, Oxford.

Akke, M., Fiala, R., Jiang, F., Patel, D. and Palmer, A.G. III (1997) *RNA* **3**, 702–709.

Allain, F.H. and Varani, G. (1995) *J. Mol. Biol.* **250**, 333–353.

Bax, A. and Davis, D.G. (1985) *J. Magn. Reson.* **63**, 207–213.

Boisbouvier, J., Brutscher, B., Pardi, A., Marion, D. and Simorre, J.P. (2000) *J. Am. Chem. Soc.* **122**, 6779–6790.

Boisbouvier, J., Brutscher, B., Simorre, J.P. and Marino, J.P. (1999) *J. Biomol. NMR* **14**, 241–252.

Boisbouvier, J., Wu, Z., Ono, A., Kainosho, M. and Bax, A. (2003) *J. Biomol. NMR* **27**, 133–142.

Borer, P.N., LaPlante, S.R., Kumar, A., Zanatta, N., Martin, A., Hakkinen, A. and Levy, G.C. (1994) *Biochemistry* **33**, 2441–2450.
Brüschweiler, R. and Wright, P.E. (1994) *J. Am. Chem. Soc.* **116**, 8426–8427.
Bryce, D.L., Boisbouvier, J. and Bax, A. (2004) *J. Am. Chem. Soc.* **126**, 10820–10821.
Case, D.A. (1999) *J. Biomol. NMR* **15**, 95–102.
Dajaegere, A.P. and Case, D.A. (1998) *J. Phys. Chem. A* **102**, 5280–5289.
Duchardt, E., Richter, C., Ohlenschlager, O., Gorlach, M., Wohnert, J. and Schwalbe H. (in preparation).
Ennifar, E., Nikulin, A., Tishchenko, S., Serganov, A., Nevskaya, N., Garber, M., Ehresmann, B., Ehresmann, C., Nikonov, S. and Dumas, P. (2000) *J. Mol. Biol.* **304**, 35–42.
Farrow, N.A., Muhandiram, R., Singer, A.U., Pascal, S.M., Kay, C.M., Gish, G., Shoelson, S.E., Pawson, T., Forman-Kay, J.D. and Kay, L.E. (1994) *Biochemistry* **33**, 5984–6003.
Farrow, N.A., Zhang, O., Szabo, A., Torchia, D.A. and Kay, L.E. (1995) *J. Biomol. NMR* **6**, 153–162.
Fernandes, M.X., Ortega, A., Martinez, M.C.L. and Torre, J.G.de la (2002) *Nucleic Acids Res.* **30**, 1782–1788.
Fiala, R., Czernek, J. and Sklenar, V. (2000) *J. Biomol. NMR* **16**, 291–302.
Garcia de la Torre, J., Huertas, M.L. and Carrasco, B. (2000) *J. Magn. Reson.* **147**, 138–146.
Gaudin, F., Paquet, F., Chanteloup, L., Beau, J.M., Nguyen, T.T. and Lancelot, G. (1995) *J. Biomol. NMR* **5**, 49–58.
Hall, K.B. and Tang, C. (1998) *Biochemistry* **37**, 9323–9332.
Ishima, R. and Nagayama, K. (1995) *J. Magn. Reson.* B **108,** 73–76.
Kay, L.E., Nicholson, L.K., Delaglio, F., Bax, A. and Torchia, D.A. (1992) *J. Magn. Reson.* **97**, 359 .
King, G.C., Harper, J.W. and Xi, Z. (1995) *Meth. Enzymol.* **261**, 436–450.
Kojima, C., Ono, A., Kainosho, M. and James, T.L. (1998) *J. Magn. Reson.* **135**, 310–333.
Korzhnev, D.M., Skrynnikov, N.R., Millet, O., Torchia, D.A. and Kay, L.E. (2002) *J. Am. Chem. Soc.* **124**, 10743–10753.
Lane, A.N. (1991) *Carbohydr. Res.* **221**, 123–144.
Lipari, G. and Szabo, A. (1982a) *J. Am. Chem. Soc.* **104**, 4546–4559.
Lipari, G. and Szabo, A. (1982b) *J. Am. Chem. Soc.* **104**, 4559–4570.
Mandel, A.M., Akke, M. and Palmer, A.G. III (1995) *J. Mol. Biol.* **246**, 144–163.
Mulder, F.A.A., Graaf, R.A.de, Kaptein, R. and Boelens, R. (1998) *J. Magn. Reson.* **131**, 351–357.
Nissen, P., Hansen, J., Ban, N., Moore, P.B. and Steitz, T.A. (2000) *Science* **289**, 920–930.
Olsen, J.I., Schweizer, M.P., Walkiw, I.J., Hamill, W.D. Jr., Horton, W.J. and Grant, D.M. (1982) *Nucleic Acids Res.* **10**, 4449–4464.
Pan, Y.P. and MacKerell, A.D. (2003) *Nucleic Acids Res.* **31**, 7131–7140.
Paquet, F., Gaudin, F. and Lancelot, G. (1996) *J. Biomol. NMR* **8**, 252–260.
Peng, J.W. and Wagner, G. (1992) *Biochemistry* **31**, 8571–8586.
Schmidt, P.G., Playl, T. and Agris, P.F. (1983) *Biochemistry* **22**, 1408–1415.
Schmidt, P.G., Sierzputowska-Gracz, H. and Agris, P.F. (1987) *Biochemistry* **26**, 8529–8534.
Shajani, Z. and Varani, G. (2005) *J. Mol. Biol.* **349**, 699–715.
Sitkoff, D. and Case, D.A. (1998) *Prog. NMR Spectroscopy* **32**, 165–190.
Spielmann, H.P. (1998) *Biochemistry* **37**, 5426–5438.
Stone, M.J., Fairbrother, W.J., Palmer, A.G. III, Reizer, J., Saier, M.H. Jr. and Wright, P.E. (1992) *Biochemistry* **31**, 4394–4406.
Stueber, D. and Grant, D.M. (2002) *J. Am. Chem. Soc.* **124**, 10539–10551.
Tjandra, N., Feller, S.E., Pastor, R.W. and Bax, A. (1995) *J. Am. Chem. Soc.* **117**, 12562–12566.
Vallurupalli, P. and Kay, L.E. (2005) *J. Am. Chem. Soc.* **127**, 6893–6901.
Varani, G. (1995) *Annu. Rev. Biophys. Biomol. Struct.* **24**, 379–404.
Varani, G., Cheong, C. and Tinoco, I. Jr. (1991) *Biochemistry* **30**, 3280–3289.
Wijmenga, S.S. and van Buuren, B.N.M. (1998) *Prog. Nucl. Magn. Res. Sp.* **32**, 287–38.
Williamson, J.R. and Boxer, S.G. (1989) *Biochemistry* **28**, 2819–2831.
Wimberly, B.T., Brodersen, D.E., Clemons, W.M. Jr., Morgan-Warren, R.J., Carter, A.P., Vonrhein, C., Hartsch, T. and Ramakrishnan, V. (2000) *Nature* **407**, 327–339.